[*American Mineralogist*]

Supporting Information for

[**Geochemical Characteristics of Lawsonite Blueschists in Tectonic Mélange from the Tavşanlı Zone, Turkey: Potential Constraints on the Origin of Mediterranean Potassium-rich Magmatism**]

[Yu Wang [1,2,*], Dejan Prelević [3,4] and Stephen F. Foley [2]]

[[1]State Key Laboratory of Isotope Geochemistry, Guangzhou Institute of Geochemistry, Chinese Academy of Sciences, Guangzhou 510640, China

[2]ARC Centre of Excellence for Core to Crust Fluid Systems/GEMOC; Department of Earth and Planetary Sciences, Macquarie University, NSW 2109, Australia

[3]Faculty of Mining and Geology, Belgrade University, Đušina 7, 11000 Belgrade, Serbia

[4]Institute for Geosciences, University of Mainz, Becherweg 21, Mainz 55099, Germany]

*Corresponding author

Contents of this file

Introduction

[This supporting file includes texts of analytical techniques, seven figures and seven tables, all of which are supplementary to the main paper]

S1 Analytical techniques

1.1 Major elements

Whole-rock major element compositions were determined by X-ray fluorescence spectrometry (XRF) using a Philips MagiXPRO spectrometer on fused discs, whereas the major element compositions of minerals were obtained by JEOL JXA 8900RL electron microprobe analyser (EMPA) at the Institute of Geosciences, University of Mainz, Germany, and CAMECA SX-100 electron microprobe (EMP) at the Department of Earth and Planetary Sciences, Macquarie University. Operating conditions were generally 15 kV accelerating voltage, 12 nA beam current, 1-5 μm beam diameter and 15-50 s counting time on peak.

1.2 Trace elements

All trace element data for minerals and rocks were analyzed by laser ablation-inductively coupled plasma-mass spectrometry (LA-ICP-MS) at the University of Mainz and Macquarie University. Whole-rock trace elements were analyzed in Mainz where rock powders were melted to form glass beads without any fluxing agent on an iridium strip heater in an argon atmosphere. Analyses from University of Mainz used an ArF EXCIMER laser (193 nm wavelength, NWR193 system by esi/New Wave) whereas those of Macquarie University used 266 nm Nd-YAG laser coupled to an Agilent 7500ce ICP-MS. The laser was operated at a repetition rate of 10 Hz for analyses at Mainz and 5 Hz at Macquarie, with laser energy at the sample site of 5–6 J/cm^2, allowing data collection from individual grains in polished thick sections (up to 80 μm thickness) for at least 40 s. Helium was used as carrier gas with a flow rate of 0.7 L/min at Mainz, whereas nitrogen was mixed with helium before ablated materials were introduced into the ICPMS at Macquarie. Data were measured for 60 s plus 30 s background with beam sizes of 30 μm, 50 μm and 80 μm for most minerals, and 20 μm for only a few small-grained accessory minerals. ^{29}Si and ^{44}Ca were used as the internal standards, applying the Si and Ca concentrations previously determined by electron microprobe. For calibration, NIST SRM 612 was analyzed at the beginning and after every 20 measurements on the unknown samples for analyses at Mainz while NIST 610 was chosen at Macquarie. The time-resolved signal was processed using the program GLITTER 4.4.1 (www.glitter-gemoc.com, Macquarie University, Sydney, Australia), applying the preferred values for NIST SRM 610 and 612 reported in the GeoReM database (http://georem.mpch-mainz.gwdg.de/) (Jochum et al., 2011) as the "true" concentrations to calculate the element concentrations in the samples. Analytical uncertainty (one sigma) for one spot analysis or line scan was less than 10%. During each run, the basaltic USGS BCR-2G reference glass was analyzed as an unknown to monitor accuracy and reproducibility of the analyses.

1.3 Radiogenic isotopes

Sr and Nd isotopic compositions were measured at the Max Planck Institute for Chemistry (MPIC), Mainz, Germany and Macquarie University. Sample dissolution and analytical separations were carried out under clean laboratory conditions. About 10 mg of sample powder was digested using a mixture of concentrated HNO_3 and HF acids. Pure Sr and Nd fractions were obtained using standard chromatographic methods. First, Sr and rare-earth elements (REE) were separated by cation exchange

in HCl media (resin: BioRad AG 50W-X8); Nd was further isolated from the REE fraction by cation exchange in ammonium form using α-hydroxyisobutyric acid (α-HIBA) buffered at pH of 4.5 as eluent. All isotopic measurements were performed on a ThermoFisher Triton TIMS instrument operating in static multicollection mode. Sr was loaded onto degassed tungsten filaments together with tantalum-fluoride (TaF$_5$) activator; Nd was loaded similarly and analyzed as the NdO$^+$ ion. ^{87}Sr/^{86}Sr data were internally normalized to ^{86}Sr/^{88}Sr = 0.1194 using the exponential law, and the Nd isotope data to ^{146}Nd/^{144}Nd = 0.7219 after correction for oxygen isobars and interferences. During the measurement period, NIST SRM-987 Sr and JMC-321 Nd yielded ^{87}Sr/^{86}Sr of 0.710264 ± 6 (MPIC) and 0.710259 ± 3 (Macquarie University) (2SD of 14 measurements), and 0.511841 ± 6 (MPIC) and 0.511122 ± 4 (Macquarie University) for ^{143}Nd/^{144}Nd (2SD of 15 measurements). The initial Sr and Nd isotopic compositions of the blueschists and phyllite were calculated from the published ages and measured atomic parent-daughter ratios (Table 2), using decay constants: λ^{87}Rb = 1.42 × 10-11 a-1 (Steiger and Jäger, 1977) and λ^{147}Sm = 6.54 × 10^{-12} a^{-1} (Lugmair and Marti, 1978). εNd$_{(T)}$ is calculated relative to CHUR values of ^{147}Sm/^{144}Nd = 0.1967 and ^{143}Nd/^{144}Nd = 0.512638.

Pb isotopic compositions were measured at MPIC (Table 3). Filters were cut into pieces (area = 5-20 cm^2) using ceramic scissors and were first acid-leached in 0.5 N HBr to effectively remove labile anthropogenic Pb. The filters were washed with MQ-water and then dissolved completely using a mixture of concentrated HF and HNO$_3$ acids. Following dissolution, chemical separation of the elements was carefully executed under clean laboratory conditions and blanks were monitored throughout the entire procedure. Pb was separated by anion-exchange chromatography (resin: BioRad AG1-X8, 100-200 mesh) to obtain its fraction following techniques described by Lugmair and Galer, 1992. All Pb isotopic measurements were performed by TIMS, and then corrected for mass fractionation using a triple-spike technique (Galer, 1999). During the period of measurements, NIST SRM 981 Pb standard yielded ^{206}Pb/^{204}Pb, ^{207}Pb/^{204}Pb and ^{208}Pb/^{204}Pb of 16.9407 ± 18 (2SD of 10 measurements), 15.4988 ± 17 and 36.7225 ± 40, respectively.

1.4 Raman spectroscopy

Confocal micro-Raman spectroscopy (Institute of Geosciences, University of Mainz) was used to constrain the purity of lawsonite. A Horiba Jobin Yvon LabRAM 800 high-resolution (HR) spectrometer equipped with a Si-based CCD detector (Peltier-cooled), an integrated Olympus BX41 optical microscope and an automated x − y stage, was used to record Micro-Raman spectra. A 50× long-distance objective (NA 0.55) together with a slit width of 100 μm were selected. The excitation source was a frequency-doubled Nd:YAG laser operating at 532.21 nm focused to a spot size of c.a. 2 × 2 μm. The Rayleigh radiation was obstructed using two-edge filters, whereas the scattered light was dispersed by a grating with 1800 grooves/mm; all spectra were recorded twice. The wavenumber accuracy is ±0.5 cm^{-1} with a measured spectral resolution of 0.6 cm^{-1} (FWHM of the Rayleigh line). The spectrometer was calibrated using the 520.5 cm^{-1} band of a silicon wafer. For the 3D mapping technique, particular areas of the cross section of the lawsonite grains were defined (e.g. 0.25mm × 0.25mm). Every 5 μm, a spectrum was recorded twice for 2 s in the x and y directions. Therefore, the resulting number of spectra was ca. 2500. The backgrounds of all 2500 spectra were subtracted individually with LabSpec software, which decomposed them into the respective sub-spectra via a

curve-fitting procedure. The resulting intensity of each peak was converted to a color code. Therefore, every pixel in the Raman map represents one spectrum and every color embodies an intensity (Wehrmeister et al., 2011).
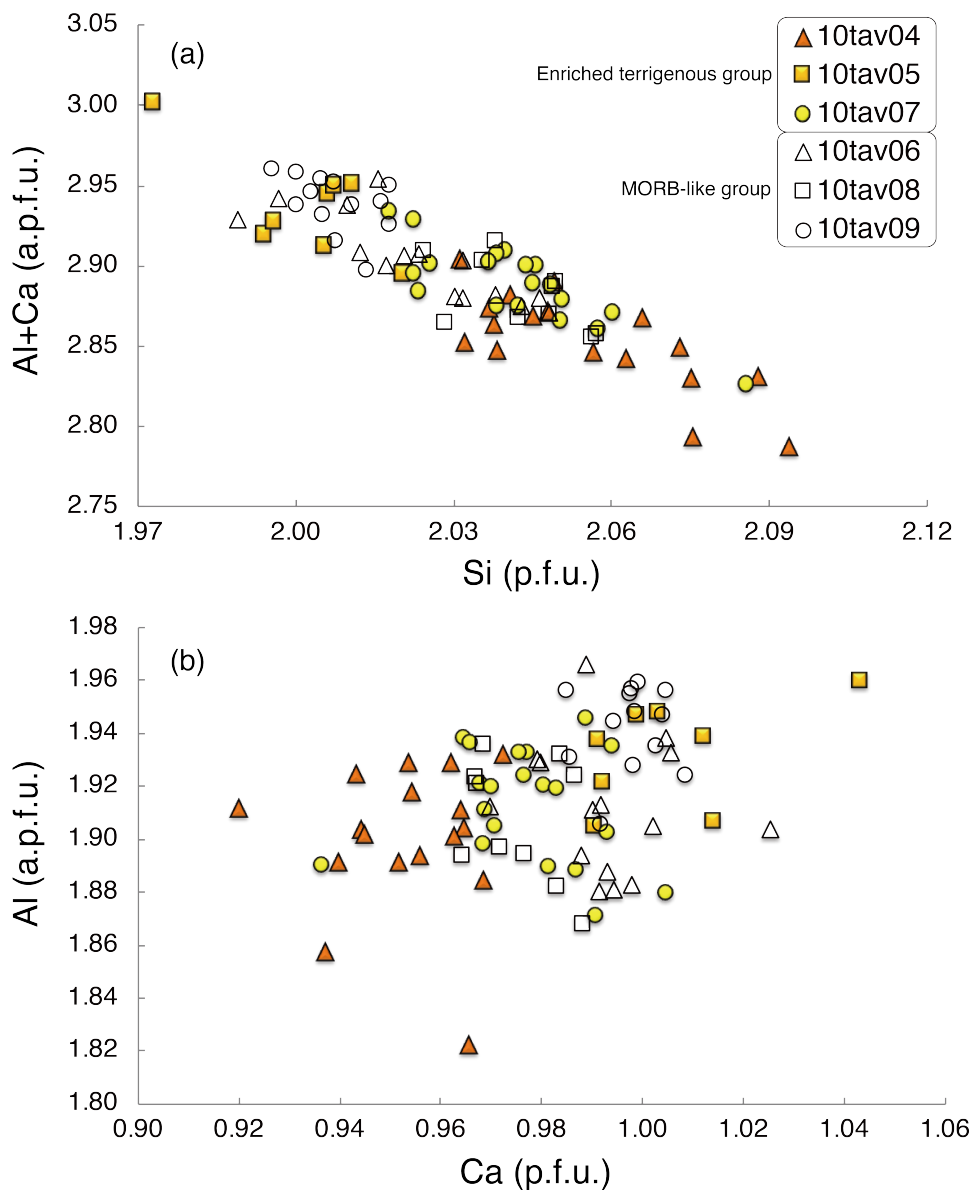
Figure S1. Variations of **(a)** Si (atomic) vs. Al + Ca (atomic) and **(b)** Ca (atomic) vs. Al (atomic) of lawsonite in the Tavşanlı zone blueschists.
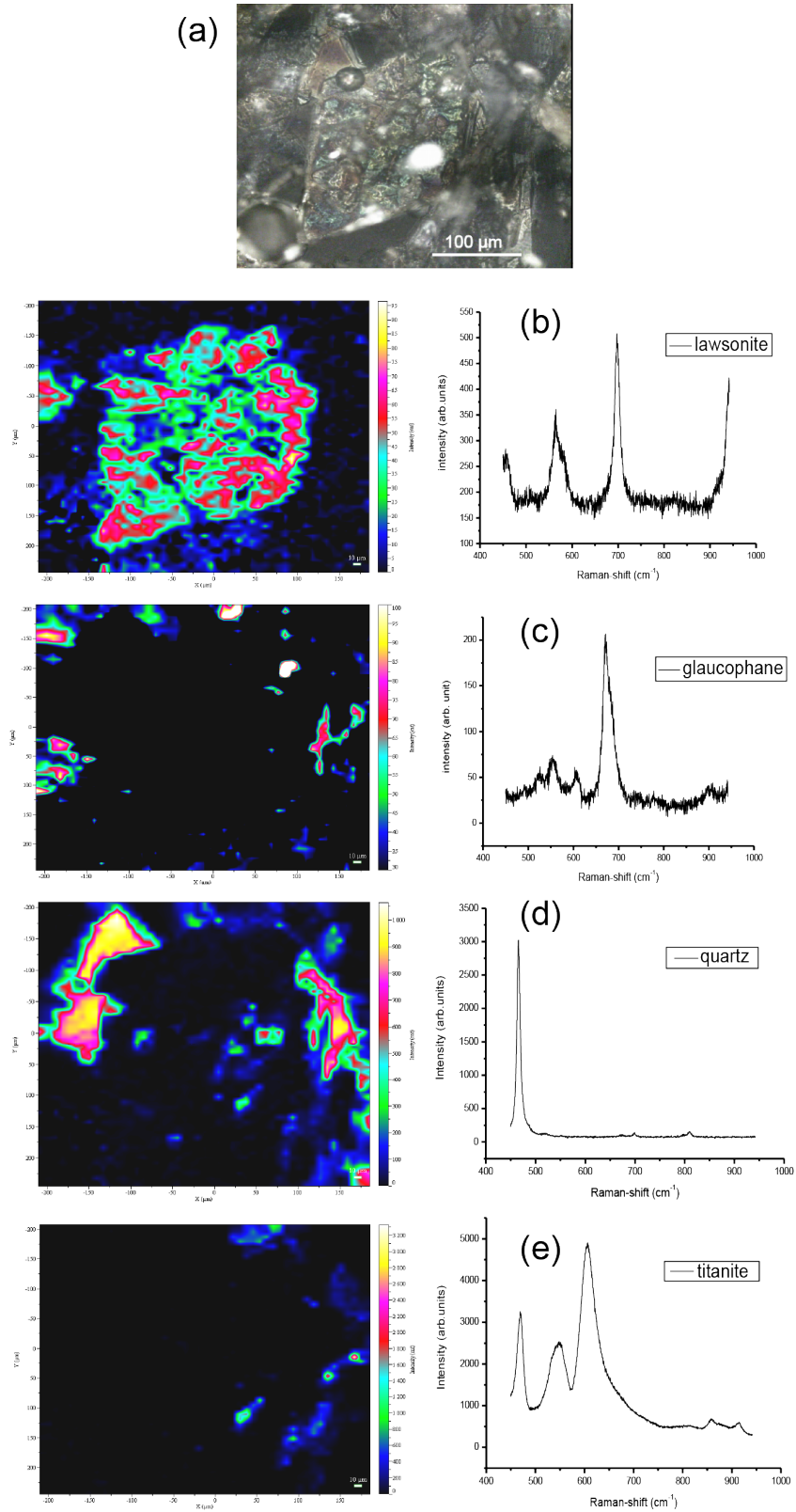
Figure S2. Confocal MicroRaman Spectroscopy 3D maps of sample 10tav07 lawsonite. **(a)** Selected sample 10tav07 lawsonite grain under microscope; **(b-e)** Representative Raman spectra of lawsonite, glaucophane, quartz and titanite, respectively.
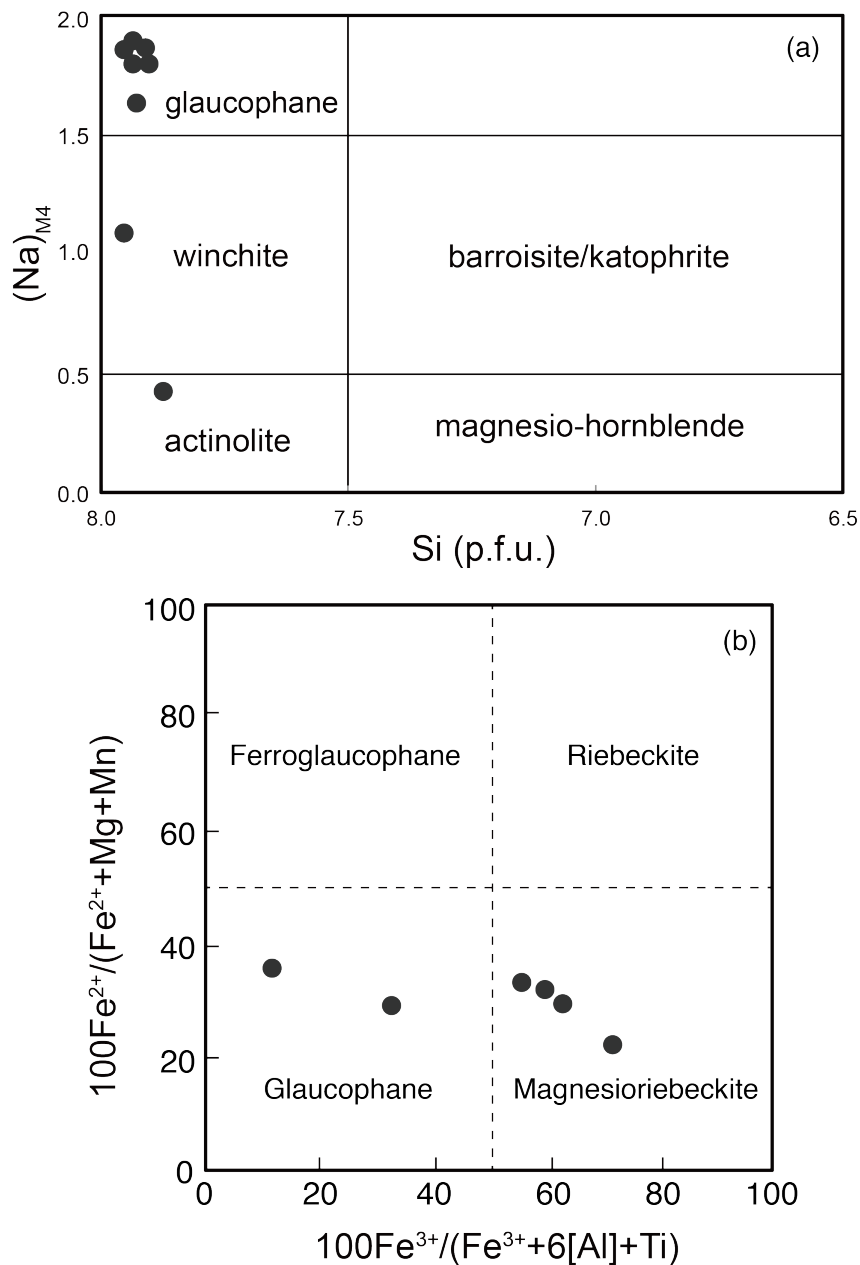
Figure S3. (a) $(Na)_{M4}$-Si (atomic) diagram for amphiboles (adapted from Leake et al., 1997; Sisson et al., 1997; Wei et al., 2009) and **(b)** glaucophane-riebeckite classification diagram for sodic amphiboles (after Deer et al., 2013) illustrating compositional variations among amphiboles.
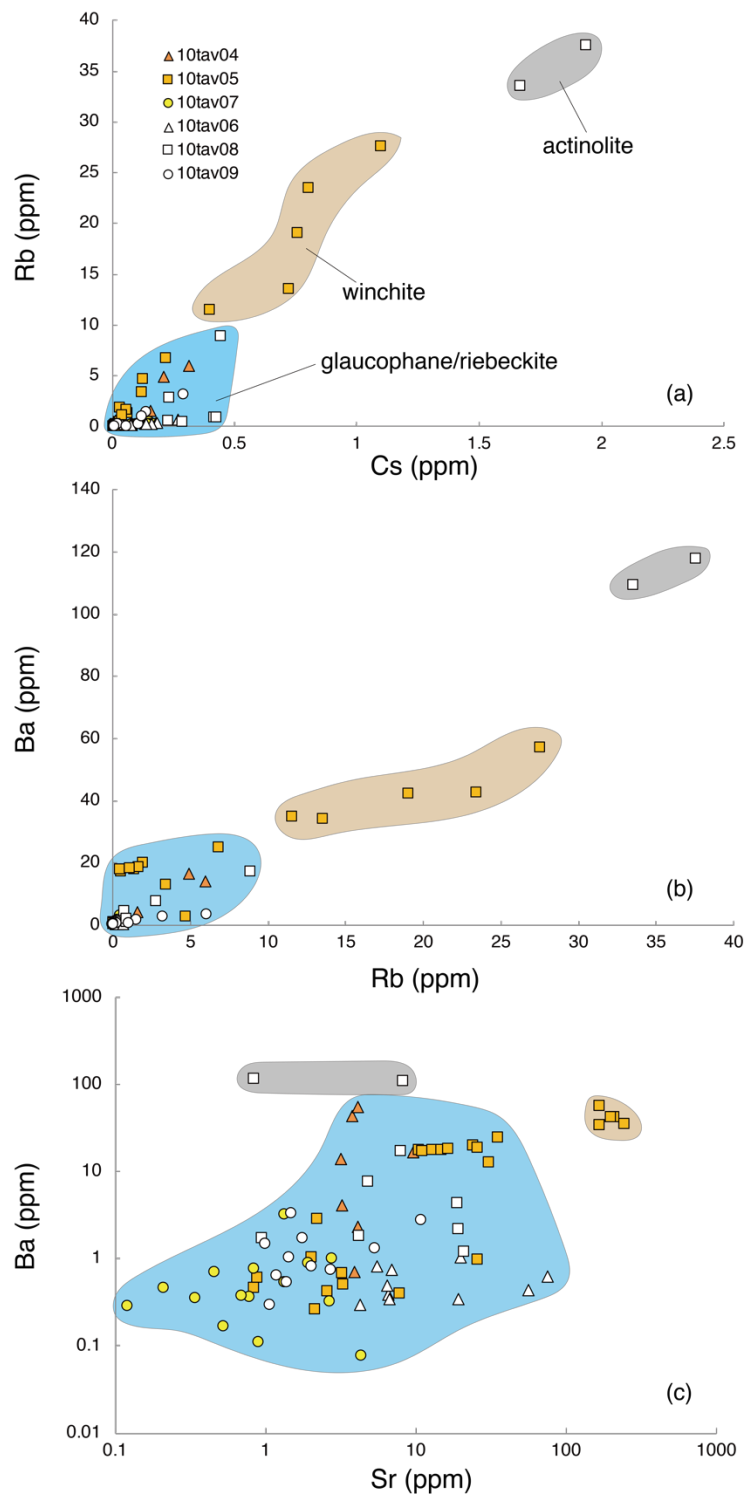
Figure S4. Variations of **(a)** Cs (ppm) vs. Rb (ppm); **(b)** Rb (ppm) vs. Ba (ppm) and **(c)** Sr (ppm) vs. Ba (ppm) for amphiboles, showing the distinctions among different amphibole facies.
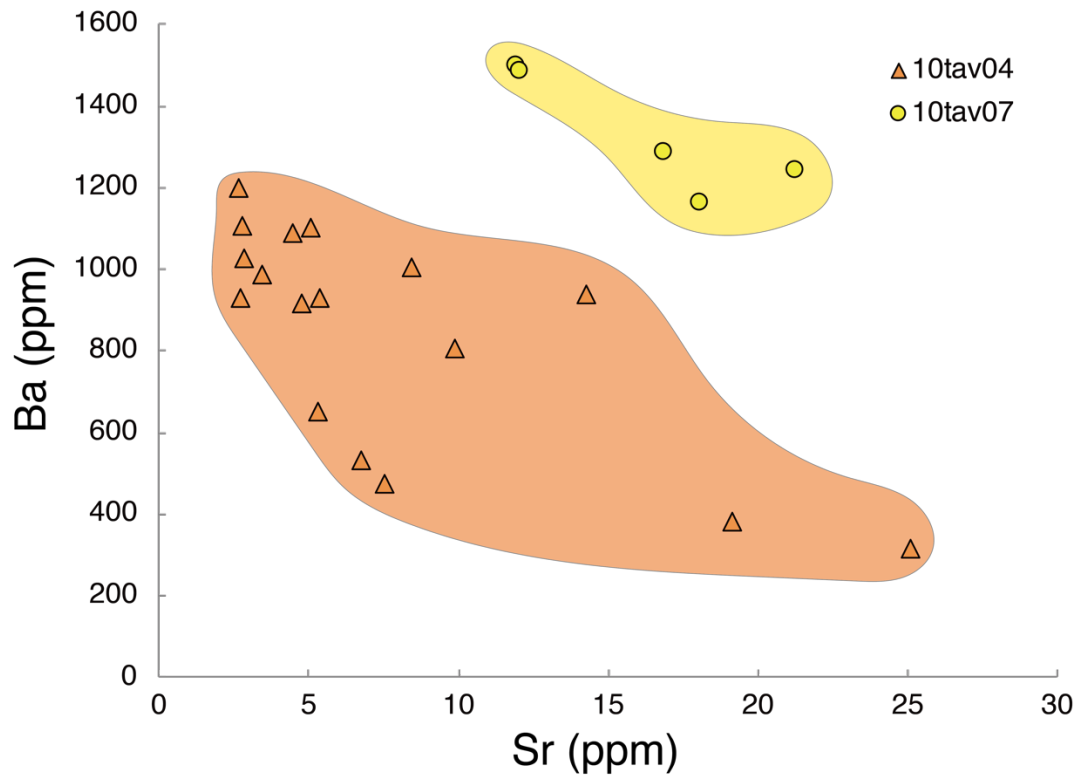
Figure S5. Variations of **(a)** Cs (ppm) vs. Rb (ppm) and **(b)** Sr (ppm) vs. Ba (ppm) for phengite.
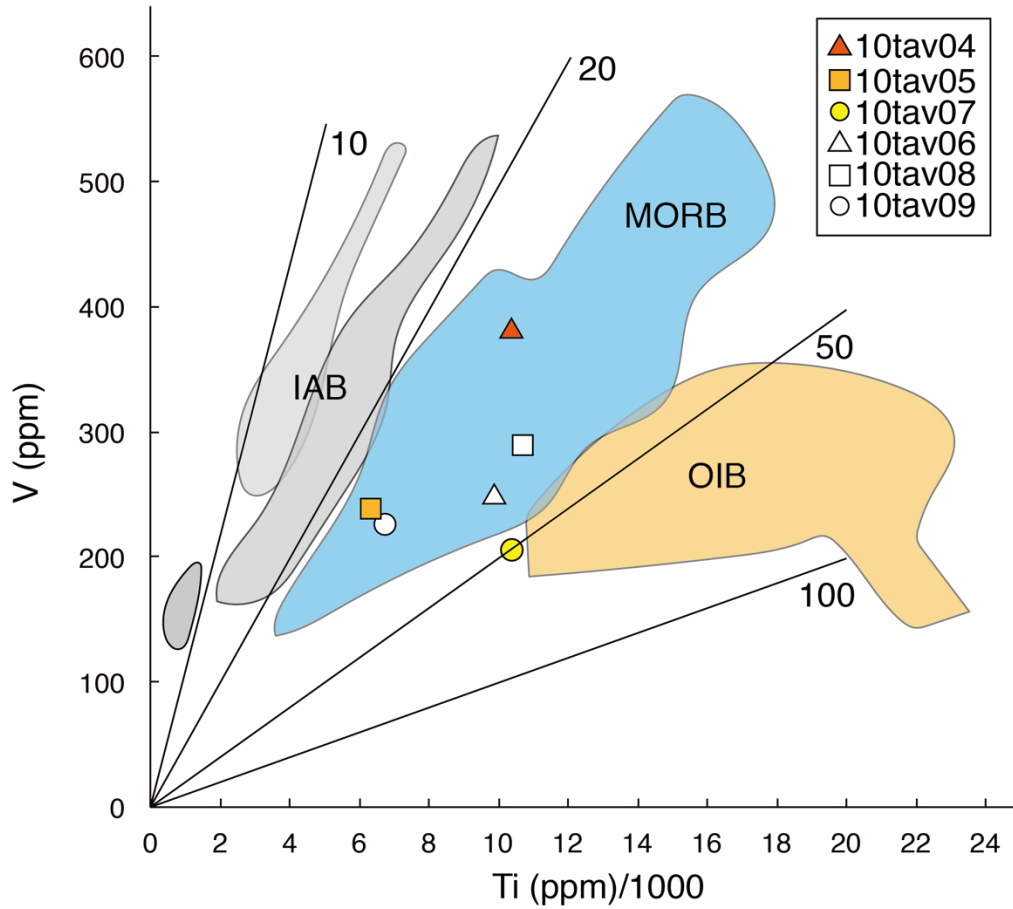
Figure S6. Ti/V plots of blueschist samples following Shervais (1982). Trend lines of constant Ti/V ratios = 10, 20, 50, and 100 added for reference. IAB (grey shaded field): Island Arc Basalt; MORB (blue shaded field): Mid-Ridge Oceanic Basalt; OIB (yellow shaded field): Oceanic Island Basalt.
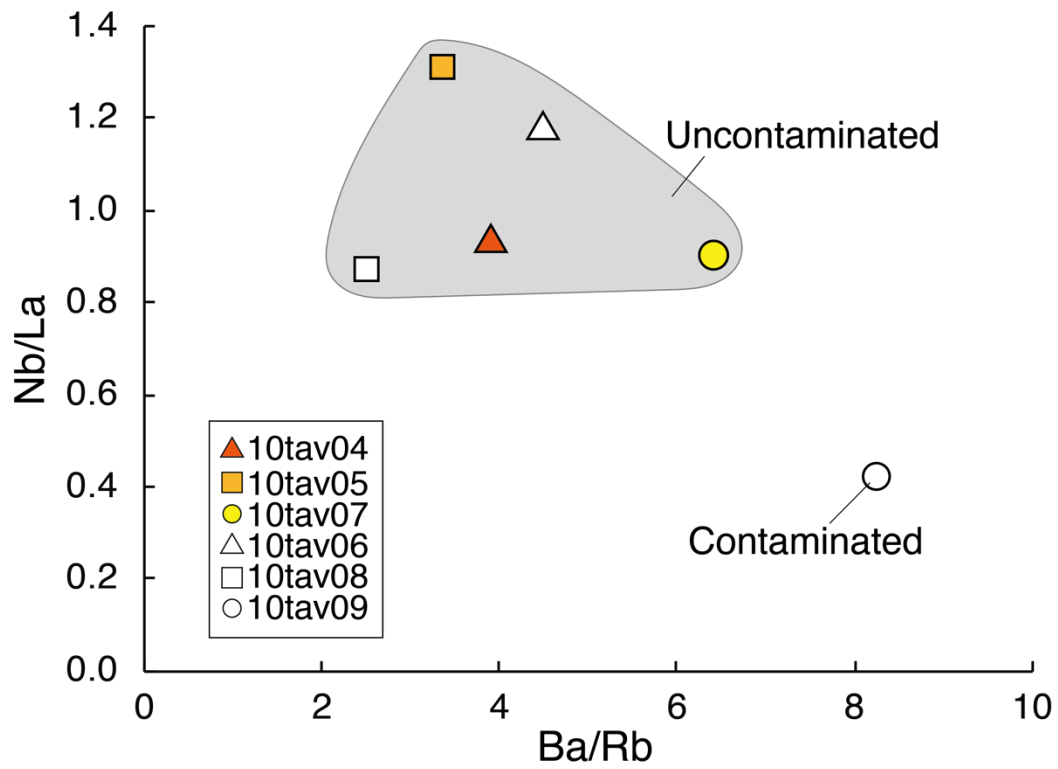
Figure S7. Ba/Rb vs Nb/La discrimination diagram of blueschist samples. Note that sample 10tav09 shows clear crustal contamination due to its much lower Nb/La (0.42) than the rest of samples.

Table S1. Major element (wt%) compositions of phengite.

Sample	10tav04	10tav05	10tav06	10tav07	10tav08	10tav09
Number of analyses	10	2	2	2	2	2
SiO_2	52.63	52.86	51.70	49.23	52.12	51.02
TiO_2	0.04	0.02	0.02	0.01	NA	NA
Al_2O_3	22.38	23.05	20.17	25.16	18.56	19.98
FeO	3.65	3.17	3.11	3.02	4.16	3.23
MnO	0.08	0.05	0.01	0.02	0.03	0.02
MgO	5.08	5.31	6.78	5.28	6.69	7.10
CaO	0.06	0.01	0.03	0.02	NA	NA
Na_2O	0.12	0.02	0.09	0.02	0.03	0.03
K_2O	10.56	10.45	10.56	10.54	10.03	10.28
Cr_2O_3	0.03	NA	0.01	0.06	0.18	0.12
Total	94.61	94.94	92.48	93.35	91.80	91.78
Si	7.13	7.10	7.17	6.76	7.31	7.14
Ti	NA	NA	NA	NA	NA	NA
Al	3.57	3.65	3.30	4.07	3.07	3.29
Fe (ii)	0.41	0.36	0.36	0.35	0.49	0.38
Mn	0.01	0.01	NA	NA	NA	NA
Mg	1.03	1.06	1.40	1.08	1.40	1.48
Ca	0.01	NA	NA	NA	NA	NA
Na	0.03	0.01	0.02	0.01	0.01	0.01
K	1.82	1.79	1.87	1.85	1.79	1.83
Total	14.01	13.97	14.13	14.12	14.06	14.14

Structural formula based on 14 cations and 22 oxygen.

Table S2. Major element (wt%) compositions of titanite.

Sample	10tav04	10tav05	10tav06	10tav07	10tav08	10tav09
Number of analyses	13	2	14	13	2	17
SiO_2	30.83	30.54	30.60	30.47	28.11	30.67
TiO_2	36.82	38.07	37.96	39.05	34.97	38.52
Al_2O_3	1.65	1.56	1.91	1.21	2.09	1.55
FeO	1.70	1.23	0.82	0.53	3.04	1.02
MnO	0.04	0.08	0.06	0.07	0.15	0.04
MgO	0.44	0.52	0.02	0.01	2.26	0.02
CaO	26.88	27.17	27.97	28.48	25.09	28.24
Na_2O	0.21	0.02	0.05	0.03	0.21	0.02
K_2O	0.13	0.11	NA	0.01	NA	NA
Cr_2O_3	0.03	0.05	0.01	0.02	0.08	0.03
Total	98.73	99.34	99.40	99.87	96.03	100.07

Table S3. Major element (wt%) compositions of chlorite, Mn-garnet and clinopyroxene. Cpx: clinopyroxene

Sample	10tav04	10tav05	10tav06	10tav07	10tav08	10tav09	10tav04	10tav07
Mineral	Chlorite	Chlorite	Chlorite	Chlorite	Chlorite	Chlorite	Cpx	Mn-garnet
N	9	3	2	5	4	2	12	12
SiO_2	29.03	29.79	28.45	32.69	28.23	28.54	50.33	37.41
TiO_2	0.01	0.01	NA	NA	0.01	0.06	0.99	0.16
Al_2O_3	17.10	18.85	17.42	14.65	17.32	17.62	3.93	20.41
FeO	18.52	14.33	20.86	12.03	21.19	21.16	9.27	15.95
MnO	0.64	0.70	0.64	1.13	0.62	0.38	0.24	17.26
MgO	21.57	21.92	19.15	22.92	19.51	19.95	16.45	0.58
CaO	0.12	0.68	0.11	0.70	0.06	0.09	17.44	8.80
Na_2O	0.03	NA	0.03	0.01	0.01	NA	0.42	0.02
K_2O	0.03	0.01	NA	0.01	NA	0.01	0.01	NA
Cr_2O_3	0.01	0.05	0.06	0.04	0.13	0.06	0.29	0.06
Total	87.07	86.39	86.75	84.20	87.14	87.90	99.35	100.65

Table S4. Mean trace element compositions of glaucophane (ppm).

Sample	10tav04	10tav05	10tav06	10tav07	10tav08	10tav09
Mineral	Gln	Win	Gln	Gln	Gln	Gln
Number of analyses	11	20	11	14	11	12
Li	51	48	47	51	44	86
Sc	31	42	43	32	41	47
Ti	1503	715	8586	317	5543	207
V	231	136	193	144	186	153
Cr	70	58	216	86	452	100
Mn	1923	2333	1371	1616	3450	1694
Co	74	73	64	33	86	88
Ga	13	5.3	12	10	29	15
Rb	39	0.62	8.8	1.7	8.7	1.1
Sr	5.9	2.8	21	1.6	22	7.0
Y	2.0	0.61	8.3	1.1	12	2.6
Zr	3.1	1.5	106	140	6.5	10
Nb	0.89	1.8	3.4	0.91	2.9	0.02
Cs	1.6	0.03	0.44	0.15	0.63	0.16
Ba	137	0.81	9.5	6.3	26	1.5
La	0.17	0.24	0.35	0.61	0.40	1.30
Ce	0.41	0.47	1.0	1.2	1.2	2.8
Pr	0.06	0.05	0.23	0.24	0.22	0.40
Nd	0.46	0.21	1.3	0.89	1.4	1.8
Sm	0.29	0.07	0.58	0.21	0.86	0.46
Eu	0.07	0.02	0.21	0.04	0.41	0.18
Gd	0.20	0.06	0.90	0.16	1.4	0.51
Tb	0.05	0.02	0.17	0.02	0.28	0.08
Dy	0.47	0.11	1.2	0.18	2.5	0.44
Ho	0.09	0.03	0.33	0.04	0.54	0.09
Er	0.25	0.09	1.2	0.15	1.6	0.20
Tm	0.05	0.02	0.19	0.03	0.27	0.03
Yb	0.25	0.16	1.8	0.25	1.4	0.21
Lu	0.02	0.03	0.33	0.05	0.19	0.04
Hf	0.38	0.16	3.2	2.9	0.30	0.33
Ta	0.08	0.09	0.23	0.06	0.22	0.01
Pb	34	38	17	3.3	48	12
Th	0.03	0.04	0.05	1.5	0.06	0.03
U	0.02	0.03	0.07	0.26	0.12	0.12

Mg-hbl: magnesio-hornblende; Gln: glaucophane; Win: winchite.

Table S5. Mean trace element compositions of titanite (ppm).

Sample	10tav04	10tav05	10tav06	10tav07	10tav08	10tav09
Number of analyses	3	2	28	36	15	9
Li	8.6	3.4	10	4.3	19	12
Sc	3.1	82	18	5.2	36	14
Ti	151566	186916	185582	234948	200397	206374
V	385	322	443	325	301	315
Cr	31	230	199	153	270	165
Mn	670	297	762	773	1502	535
Co	18	4.9	16	3.6	28	15
Ga	6.5	6.9	5.8	2.4	8.0	3.7
Rb	29	3.1	0.89	1.9	10	1.0
Sr	20	56	20	36	26	17
Y	305	101	74	294	422	258
Zr	124	505	183	227	125	53
Nb	102	582	79	723	106	103
Cs	1.1	0.11	0.15	0.09	0.66	0.11
Ba	106	88	5.5	17	34	3.7
La	3.6	44	1.0	3.7	1.2	2.4
Ce	25	201	4.9	11	8.8	8.0
Pr	7.1	27	0.53	2.2	2.5	2.3
Nd	53	111	2.8	15	22	16
Sm	31	30	1.80	11	20	12
Eu	12	12	0.80	5.0	11	6.7
Gd	43	26	3.0	19	34	19
Tb	8.7	4.6	0.90	5.5	10	5.8
Dy	63	29	13	48	81	47
Ho	13	5.0	3.8	12	18	11
Er	38	12	13	38	54	34
Tm	5.0	1.7	3	6.2	8.4	5.8
Yb	30	11	22	43	57	44
Lu	2.3	0.93	2.3	4.8	6.1	4.5
Hf	2.6	13	7.1	6	4.1	2.4
Ta	5.1	33	4.6	41	6.4	5.0
Pb	74	22	133	95	44	91
Th	0.22	9	0.13	1.7	0.17	0.08
U	0.64	3.1	0.59	1.8	1.2	1.2

Table S6. Mean trace element compositions (ppm) of chlorite, phengite, aragonite and Mn-garnet.

Sample	10tav04	10tav07	10tav04	10tav09	10tav05	10tav07
Mineral	phengite	phengite	chlorite	chlorite	aragonite	Mn-garnet
Number of analyses	20	7	10	2	3	32
Li	27	18	58	91	0.15	2.0
Sc	12	15	5.5	7.8	0.59	89
Ti	1198	22245	480	48	26	5499
V	214	151	66	48	25	95
Cr	82	485	34	75	17	149
Mn	1248	843	3669	2040	41	120277
Co	41	13	122	102	0.14	12
Ga	25	25	26	22	1.4	7.4
Rb	197	179	9.7	2.7	0.03	0.84
Sr	18	19	6.5	3.5	2889	9.3
Y	3.7	50	1.8	0.24	4.5	424
Zr	7.2	16	1.5	0.21	0.04	195
Nb	0.63	62	0.28	0.01	0.02	14
Cs	8.6	3.9	0.45	0.19	0.02	0.07
Ba	800	1168	36	1.8	66	3.4
La	0.86	0.78	0.74	0.03	3.0	14
Ce	2.5	2.3	1.7	0.02	5.4	28
Pr	0.33	0.67	0.23	0.03	0.67	3.0
Nd	1.5	5.6	1.1	0.11	2.8	12
Sm	0.53	3.5	0.35	0.09	0.62	2.9
Eu	0.19	1.5	0.11	0.03	0.23	0.83
Gd	0.56	5.1	0.37	0.08	0.73	4.8
Tb	0.11	1.5	0.06	0.02	0.11	1.9
Dy	0.66	11	0.31	0.06	0.71	31
Ho	0.16	2.1	0.08	0.02	0.14	14
Er	0.49	5.6	0.20	0.05	0.36	70
Tm	0.08	0.94	0.03	0.01	0.03	15
Yb	0.45	6.0	0.21	0.08	0.19	132
Lu	0.06	0.66	0.03	0.01	0.02	23
Hf	0.35	0.74	0.12	0.05	0.02	4.8
Ta	0.09	5.6	0.02	0.01	0.01	1.0
Pb	69	16	91	18	29	32
Th	0.05	0.40	0.03	0.02	0.08	3.1
U	0.05	0.34	0.02	0.03	0.04	1.5

Table S7. Mean trace element compositions (ppm) of apatite, hematite and galena.

Sample	10tav04	10tav05	10tav06	10tav07	10tav08	10tav07	10tav05
Mineral	apatite	apatite	apatite	apatite	apatite	hematite	galena
Number of analyses	16	2	8	5	12	1	1
Li	12	9.4	75	0.21	4.3	0.17	31
Sc	21	1.1	117	0.40	6.8	3.9	39
Ti	826	333	14110	113	1047	169	187
V	92	70	317	1.8	21	7310	146
Cr	24	197	714	5.0	29	62	132
Mn	2119	1015	3481	454	816	12724	1526
Co	23	18	123	0.76	8.7	21939	52
Ga	8.8	7.0	19	0.70	3.3	14	7.9
Rb	16	4.0	0.38	0.53	0.66	0.29	0.12
Sr	1890	388	93	518	215	213	48
Y	682	41	34	86	135	60	6.1
Zr	17	0.08	106	19	5.9	27	0.76
Nb	0.81	0.85	5.5	0.38	0.58	2.7	0.16
Cs	0.84	0.19	0.17	0.07	0.05	0.02	0.05
Ba	53	10	10	6.1	7.0	714	1.6
La	27	6.6	3.1	2.1	4.5	1241	5.7
Ce	90	14	3.4	5.5	14	201	11
Pr	15	1.7	0.80	1.1	2.3	159	1.1
Nd	77	6.6	4.2	6.3	14	471	4.2
Sm	33	1.9	1.7	3.1	6.7	54	0.64
Eu	13	0.84	0.63	1.2	3.3	11	0.34
Gd	57	3.1	2.6	5.4	12	29	0.91
Tb	13	0.58	0.58	1.2	2.6	3.2	0.18
Dy	106	4.7	4.6	10	19	15	1.1
Ho	27	1.4	1.2	2.9	4.8	2.7	0.20
Er	85	4.9	4.1	10	15	7.4	0.62
Tm	10	0.71	0.71	1.5	2.1	1.0	0.06
Yb	55	4.8	5.4	8.1	14	7.2	0.39
Lu	6.2	0.63	0.89	1.2	2.3	1.2	0.06
Hf	0.68	0.03	3.4	0.61	0.19	0.45	0.19
Ta	0.12	0.05	0.39	0.05	0.04	0.02	0.02
Pb	120	30	29	11	6.1	602	115069
Th	0.17	0.36	13	0.35	0.15	18	0.28
U	0.16	0.13	1.5	0.08	0.14	17	0.06